Journal of Catalysis **212,** 1–9 (2002)
doi:10.1006/jcat.2002.3760

Nanosize Ti–W Mixed Oxides: Effect of Doping Level in the Photocatalytic Degradation of Toluene Using Sunlight-Type Excitation

A. Fuerte,* M. D. Hernández-Alonso,* A. J. Maira,* A. Martínez-Arias,* M. Fernández-García,*,[1] J. C. Conesa,* J. Soria,* and G. Munuera†

*Instituto de Catálisis y Petroleoquímica (CSIC), Campus Cantoblanco, 28049-Madrid, Spain; and †Instituto de Ciencia de Materiales de Sevilla (Centro Mixto Universidad Sevilla-CSIC), Avda. Américo Vespucio s/n, Isla de la Cartuja, 41092-Sevilla, Spain

Received March 13, 2002; revised July 9, 2002; accepted July 30, 2002

In this report we investigate the behavior of nanosize Ti–W mixed oxides with anatase structure in the photoelimination of toluene using sunlight-type excitation. These systems were prepared by a microemulsion method and their physicochemical properties characterized by a multitechnique approach using X-ray diffraction and photoelectron spectroscopy, as well as Raman, infrared and UV–vis spectroscopies. The preparation method allows the incorporation of up to ca. 20 at.% of W in substitutional positions of the anatase network. The photoactivity of the substitutionally disordered Ti–W mixed oxides grows in parallel with the W content of the material and improves the performance of a single anatase sample prepared in a similar way and also that of the Degussa P25 material. The chemical/physical basis of such behavior is discussed in light of the characterization results. © 2002 Elsevier Science (USA)

Key Words: **photocatalysis; binary mixed oxides; anatase; Ti–W mixed oxides; visible light absorption; pollutant and toluene mineralization and degradation.**

INTRODUCTION

Photocatalytic destruction of organic pollutants in the presence of TiO_2 appears to be a viable decontamination process of widespread application, no matter the state (gas or liquid) or chemical nature of the process target (1, 2). However, its technological application seems limited by several factors, the most restrictive of which is the need for an ultraviolet (UV) excitation source. The efficient use of solar light, or in other words light from the visible region of the spectrum, may then appear to be an appealing challenge for developing the future generation of photocatalytic materials.

The study of TiO_2 doping at low concentrations, e.g., below a few atomic percent, is not new and wide surveys of Ti–M mixed oxide photoreactivity using UV light have been reported (see, for example, Ref. (3)). Also, recently Li, V, and Cr substitutional doping of TiO_2 anatase was shown to yield materials able to absorb visible light and having good/enhanced activity for phenol (4) or NO_x photoelimination (5, 6). Theoretical analysis of substitutional doping shows, however, that the threshold energy of radiation absorption decreases with increasing dopant concentration; in fact, for a random distribution of substitutional acceptors/donors of charge dopants, a gaussianlike density of states appears at the upper/lower part of the valence/conduction band (7). The corresponding density of states is directly proportional to the dopant concentration, thus giving a clear tool for managing visible light absorption. Nevertheless, high doping concentrations may have detrimental effects because tunneling between trapped charge carriers makes a significant contribution to (charge) recombination, so that the photocatalytic rate constant typically decreases with the shortening of the electron-hole pair distance, e.g., with a growing level of dopant (8).

We recently explored the doping of the anatase structure using high concentrations of nine different dopants and showed that W can be one of the best options for toluene photodegradation using sunlight-type excitation (9). In that case, a microemulsion preparation method was used since it facilitates, as much as possible, the homogeneity of chemical composition at a nanoscale level as well as the production of particles with a narrow size distribution (10). Nanosize materials can have enhanced photochemical properties with respect to bulk specimens because they minimize band bending, facilitating the presence of both types of charge carriers (electron and holes) at the surface of titania (*n*-type conductor), being thus readily available for both reductive and oxidizing steps of the photocatalytic process (11, 12).

In this work we study the influence of the doping level of W on the photoactivity of nanosize anatase-type samples for the mineralization of toluene. The study is intended to give a picture of the physicochemical characteristics of the materials and the influence of such parameters on the mentioned reaction, paying particular attention to the high load region of doping. It will be shown that our careful preparation method allows insertion of up to ca. 20 at.% of W in substitutional positions of the anatase structure. To

[1] To whom correspondence should be addressed. Fax: + 34-91-585-4760. E-mail: m.fernandez@icp.csic.es.

0021-9517/02 $35.00

assist in interpreting the photocatalytic behavior of these highly loaded samples, reference systems consisting of W low-loaded and W-deposited specimens were also analyzed. Toluene photoactivation was chosen to test activity, as it is thought to be an important constituent of anthropogenic emissions in urban atmospheres. Additionally, its photooxidation is a very demanding reaction and thus constitutes a tough chemical test of the potential of the Ti–W systems in the photoelimination of organic pollutants.

EXPERIMENTAL PROCEDURE

Mixed Oxide Synthesis and Characterization

Materials were prepared by addition of Ti tetraisopropoxide to an inverse emulsion containing an aqueous solution (0.5 M) of ammonium tungsten oxide dispersed in *n*-heptane, using Triton X-100 (Aldrich) as surfactant and hexanol as cosurfactant. The resulting mixture was stirred for 24 h, centrifuged, decanted, rinsed with methanol, and calcined under air for 2 h at 723 K. Ti:W composition was analyzed by using inductively coupled plasma and atomic absorption (ICP–AAS) and the W atomic percentage present in the sample was used to label them (see Table 1). Reference samples were produced by deposition–precipitation of W (by slow addition of acetic acid to a reverse microemulsion containing the above-mentioned tungsten salt) over TiO_2 (prepared by microemulsion in a previous step) and are denoted as W*xx* TiO_2, where *xx* describes the weight percentage of W as WO_3. The BET surface areas were measured by nitrogen physisorption (Micromeritics ASAP 2010). Particle sizes were measured with XRD using the Scherrer equation and validated in key cases with transmission electron microscopy. Lattice parameters were calculated by fitting using Pearson VII functions and the Winfit! Program (© S. Kumm; http//www.geol.unerlangen.de). XRD profiles were obtained with a Seifert diffractometer using Ni-filtered Cu K_α radiation. Samples for transmission electron microscopy (TEM) were prepared by crushing them in an agate mortar, dispersing them in isobutanol, and depositing them on perforated carbon films supported on copper grids. TEM data were obtained on a JEOL 2000 FX II system (with 3.1-Å point resolution) equipped with a LINK probe for energy-dispersive spectroscopy (EDS) analysis. UV–visible diffuse reflectance spectroscopy experiments were performed with a Shimadzu UV2100 apparatus and Raman data were acquired using a Bruker RFS-100 FT-Raman spectrometer.

Photoelectron spectra were recorded with a Leybold–Heraeus spectrometer equipped with an EA-200 hemispherical electron multichannel analyzer (from Specs) and a 120-W, 30-mA, Al $K\alpha$ (1486.6 eV) X-ray source. A Pentium III PC was used for controlling the instrument and recording the spectra. The powder samples (200 mg) were slightly pressed into small (4×4 mm^2) pellets and then mounted on a sample rod and introduced into the pretreatment chamber, where they were outgassed at 423 K for 1 h, until a pressure below 2×10^{-8} Torr (1 Torr = 133.33 N/m^2) was achieved; they were then moved into the ion-pumped analysis chamber, where they were further outgassed until a pressure below 2×10^{-9} Torr was attained (2–3 h). The C 1s signal at 284.6 eV was used as reference for peak energy calibration. The W 4f peak overlaps with the Ti $3p_{3/2}$ one; the corresponding spectral region was then fitted using the UNIFIT. 2 program (13), as formed by a doublet (with relative intensity and spin–orbit coupling constant fixed to the WO_3 values) and a singlet (for Ti $3p_{3/2}$). Ti-related corrections correspond to 5–10% of the intensity except in the W 0.9 case, where the area calculated for the W contribution can only be considered indicative.

Photoreactivity Measurements

Activity and selectivity for the gas-phase photooxidation of toluene were tested in a continuous-flow annular photoreactor (described in Ref. (12)) containing ca. 100 mg of photocatalyst as a thin layer coating on a pyrex tube. The reacting mixture (100 ml/min) was prepared by injecting toluene (Panreac, Spectroscopic grade) into a wet oxygen flow before insertion at room temperature into the photoreactor. After flowing the mixture for 1 h (control test) in the dark, the catalyst was irradiated by four fluorescent daylight lamps (6W, Sylvania F6W/D) with a radiation spectrum emulating sunlight (UV content of 3%), symmetrically positioned outside the photoreactor. Reaction rates were taken in (vide supra) steady-state conditions, typically 3 to 4 h after starting irradiation. No change in activity was detected for all samples within the next 6 h. The concentration of reactants and products was analyzed using an online gas chromatograph (HP G1800C) equipped with a HP5 capillary column (0.25-mm. I.D. × 30 m) and an electron ionization detector.

TABLE 1

Main Characterization Results of Ti–W Mixed Oxide and Reference Samples

Sample	W atomic percentage[a]	BET surface area ($m^2\ g^{-1}$)	Crystal size (nm)
TiO_2	—	106	8.5
WO_3	—	4	28
W 27	27	81	—[b]
W 19	19	122	5.0
W 14	14	108	8.5
W 0.9	0.9	75	10
W 3.4 TiO_2	1.2	51	12

[a] Cation basis ($100 \times W/(W + Ti)$) by ICP–AAS.
[b] Not measurable by XRD with confidence.

Fourier Transform Infrared (FTIR) Measurements

For the infrared (IR) experiments, a Nicolet 5ZDX-FTIR spectrometer equipped with a MCT detector (4-cm^{-1} resolution) was used. The samples were pressed into thin wafers (15 mg/cm^2) and placed in an IR Pyrex cell equipped with NaCl windows and greaseless stopcocks. The cell could be evacuated by connecting to a conventional vacuum line (residual pressure: 1×10^{-4} Torr). For irradiating the wafer, the IR cell was introduced into an apparatus (lamp type and geometrical setup) similar to that used for performing the photoreactivity tests.

The IR spectra of two different samples (TiO_2, prepared by microemulsion, and W 19) were recorded after the following treatments performed at room temperature: (i) evacuation for 2 h; (ii) dosing of 5 Torr of toluene (Panreac, Spectroscopic grade; distilled in vacuum before use) into the IR cell and subsequent introduction of 50 Torr of oxygen; (iii) irradiation for 1 h; and (iv) evacuation of the sample for 15 min.

RESULTS

In Table 1 we report the main characteristics of the materials synthesized; the microemulsion method is able to obtain Ti–W mixed oxides after 723 K calcination with surface areas ca. 75–125 $m^2\ g^{-1}$ and with particle sizes ranging from 5 to 12 nm. As mentioned, particle size was estimated from XRD (Table 1, Fig. 1) and confirmed by using TEM (see, for example, Fig. 2). The TEM image also illustrates the precise control of particle size (narrow size distribution) obtained upon employment of the microemulsion preparation method.

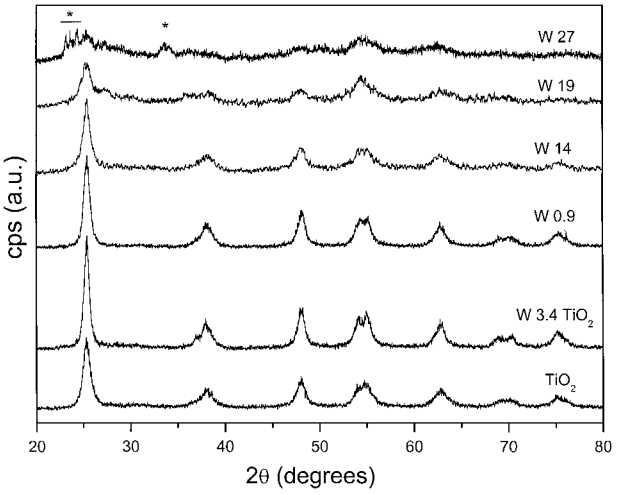

FIG. 1. XRD spectra of Ti–W specimens and references. ∗, WO_3 peaks.

X-ray diffraction (Fig. 1) and Raman spectroscopy (Fig. 3) of the systems give evidence that all samples contain titania in an anatase-type structure, with the crystallinity of the material decreasing with the W content. No significant

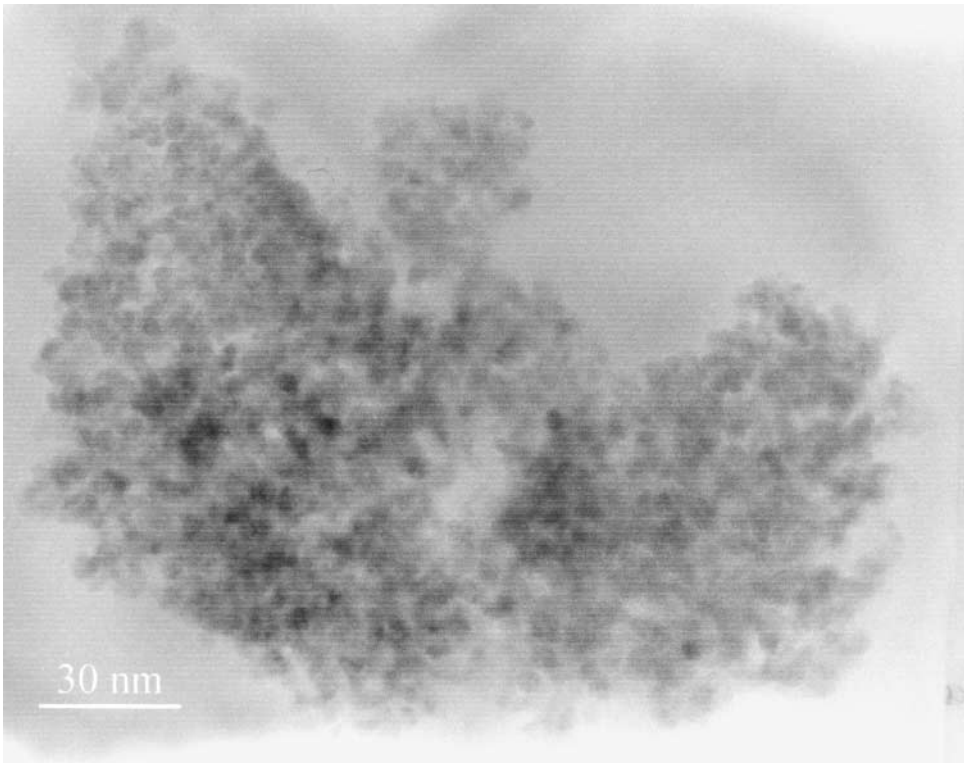

FIG. 2. Bright-field TEM image of the W 19 sample.

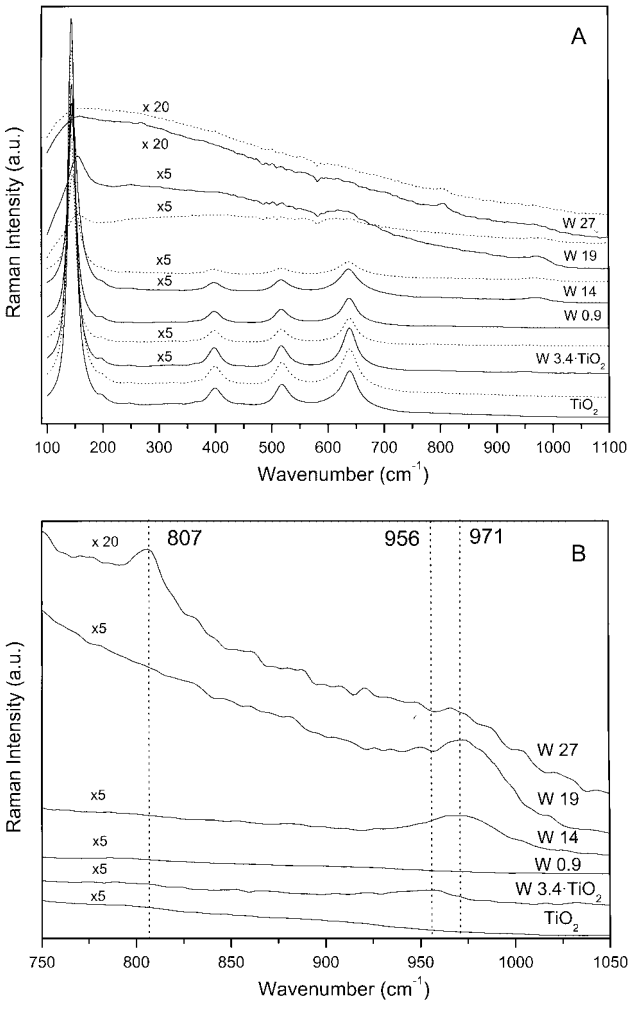

FIG. 3. Raman spectra (A) and detail (B) of Ti–W specimens. (Solid line) Calcined samples; (dashed line) postreaction samples.

differences are encountered from XRD results concerning postreaction specimens (not shown). Cell parameters and volume are summarized in Table 2. The TiO_2 XRD results are in good agreement with literature reports (JCPDS-84-1286 (14)) and show that the presence of W mainly produces a decrease in c parameter and cell volume. The absence of

TABLE 2

XRD-Derived Anatase-Type Lattice Parameters of Reference TiO_2 and Ti–W Samples

Sample	Cell parameters (Å)		Cell volume (Å^3)
	$a = b$	c	
W 19	3.7906 ± 0.0022	9.274 ± 0.007	133.2_5
W 14	3.7842 ± 0.0007	9.468 ± 0.003	135.6
W 0.9	3.7804 ± 0.0006	9.512 ± 0.003	136.0
TiO_2	3.7830 ± 0.0008	9.511 ± 0.001	136.1

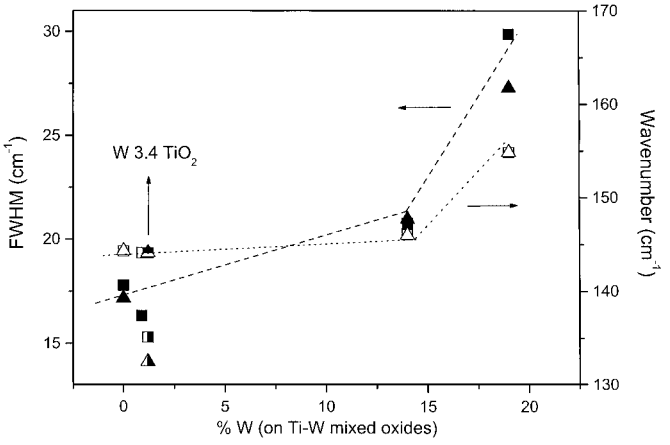

FIG. 4. FWHM and peak position of the E_g Raman mode of the anatase-type structure present in Ti–W and reference samples. (Squares) Calcined samples; (triangles) postreaction samples. (Closed symbols) FWHM; (open symbols) energy position. (Dashed lines) Used only as a reference guide for the aids.

well-developed, bulklike hereto-atom single-oxide phases was confirmed using both techniques, with the exception of the W 27 case, where a mixture of orthorhombic WO_3 (3.9% weight) and a Ti-containing anatase-type structure was obtained. This weight percentage was estimated after recording XRD spectra of physical mixtures of the W 27 material and the orthorhombic WO_3 single oxide prepared by microemulsion (which displays an average particle size similar to that present in the mentioned sample, according to XRD results). Analysis of the FWHM and energy position of the E_g anatase Raman mode as a function of the W at.% present in the materials is depicted in Fig. 4. The figure gives evidence of the presence of a break point in both observables for a W content around 15 at.%.

Surface characteristics of the Ti–W samples were followed by using the Raman band at ca. 970 cm^{-1}, corresponding to W=O bond stretching (15), which suggests that materials with a 14–19 at.% level of doping have surface wolframyl moities (Fig. 3B). Notice that this (W=O) stretch displays a different frequency in the Ti–W and W-supported specimens. No other W species is detected for these samples; however, an additional Raman band at 807 cm^{-1} appears on the W 27 spectra. This contribution is characteristic of the W=O bond stretching of well-developed WO_3 single-oxide particles (15), in accordance with XRD results. For the W 0.9 sample, there is an absence of the above-mentioned W-related Raman peaks; this, however, is common for anatase samples with doping levels close to 1 at.% (see, for example, Ref. (16)). On the other hand, no significant W or Ti segregation was detected using XPS, as shown by the data displayed in Fig. 5. XPS also shows the exclusive (or highly dominant) presence of Ti(IV) and W(VI) species, with binding energies of 458.5 ± 0.1(Ti $2p_{3/2}$) and 35.8 ± 0.2 (W $4f_{7/2}$) eV, respectively, for all samples studied (17).

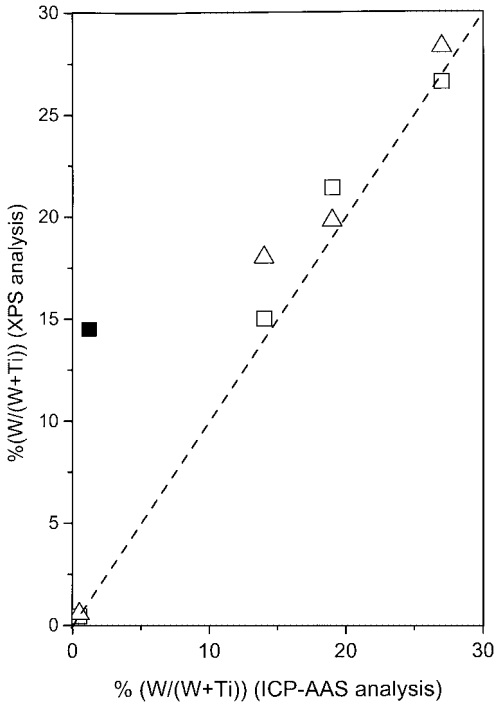

FIG. 5. W atomic percentage measured by XPS plotted vs the same observable measured by atomic absorption (AAS). (Squares) Calcined samples; (triangles) postreaction samples. (Closed symbol) W 3.4 TiO_2 sample. (Dashed line) The bisecting line of the graph.

The presence of W also has influence on the electronic properties of the material synthesized. Figure 6 shows the UV–vis-DRS spectra of the samples, which display an absorption threshold onset that continuously shifts to the visible region with the W content of the calcined material. This redshift is also visible for the W-deposited W 3.4 TiO_2 reference sample. Also, a tail is clearly observed in the W 27 specimen, evidencing again the presence of WO_3 entities.

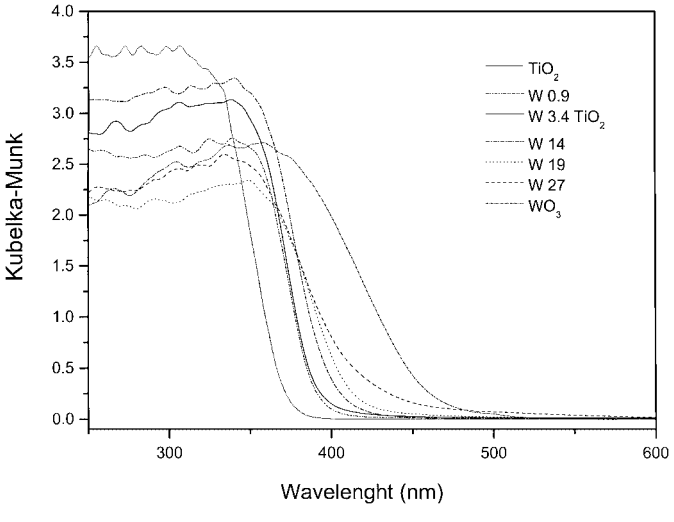

FIG. 6. UV–vis spectra of calcined Ti–W specimens and references.

TABLE 3

Reaction Rate of Ti–W Catalyst and Reference Materials for the Gas-Phase Photooxidation of Toluene under Sunlight-Type Excitation

Catalyst	Rate 10^{10} ($mol \cdot s^{-1} \cdot m^{-2}$)	Rate 10^{8} ($mol \cdot s^{-1} \cdot g^{-1}$)	Selectivity[a] (%)
TiO_2	1.0	1.0	5
TiO_2 P25 (Degussa)	0.65	0.35	14
WO_3	4.6	0.1	100
W 27	2.9	2.2	13
W 19	3.3	4.0	13
W 14	1.8	1.9	16
W 0.9	1.2	0.9	7
W 3.4 TiO_2	1.4	0.8	15

[a] To benzaldehyde (the only other detectable product being CO_2).

No significant differences are encountered from results concerning postreaction specimens (not shown).

Photocatalytic activity of the Ti–W mixed oxides in the gas-phase toluene mineralization is presented in Table 3. Also included in this table is the activity of some single oxides (TiO_2, WO_3) prepared by microemulsion and the commercial (anatase + rutile) P25 (Degussa) material. Analysis of Table 3 gives evidence of an enhanced toluene mineralization photoactivity upon W doping. Result of the Ti–W series shows that photoactivity increases with W content, exhibiting a maximum for the W 19 specimen; it is also appreciated that the presence of W favors selectivity to benzaldehyde to a small extent, although no specific trend can be established in this respect. Samples with small quantities of W, either deposited onto or into the anatase phase, can exhibit an improved performance with respect to titania, although the reaction rate increase is very modest or absent.

Using EPR, a weak signal of symmetric lineshape at $g = 2.003$ and $\Delta H_{pp} \approx 9$ G, probably arising from surface or near-surface (as its amplitude significantly decreases when recording the spectrum under air atmosphere) toluene-derived carbonaceous species, was detected for W 14 and W 19 samples after use in the reaction, but, unfortunately, no correlation was observed in this experiment between signal intensity and the amount of W cations present in the samples.

An infrared study was carried out for the W 19 and TiO_2 samples (Fig. 7A and B, respectively). In order to reveal more clearly changes induced on the catalyst surface upon each treatment of the sequence described under results, each specturm was subtracted from the subsequent one. All the FTIR spectra display a very broad absorption in the 3800- to 2800-cm^{-1} range, which is attributed to interacting OH groups (i.e., affected by hydrogen bonds) and adsorbed molecular water. The large intensity of this absorption, which produces the (near) saturation of this area of the spectra, is mainly due to the high surface area displayed by the catalysts. Since it was not possible to obtain

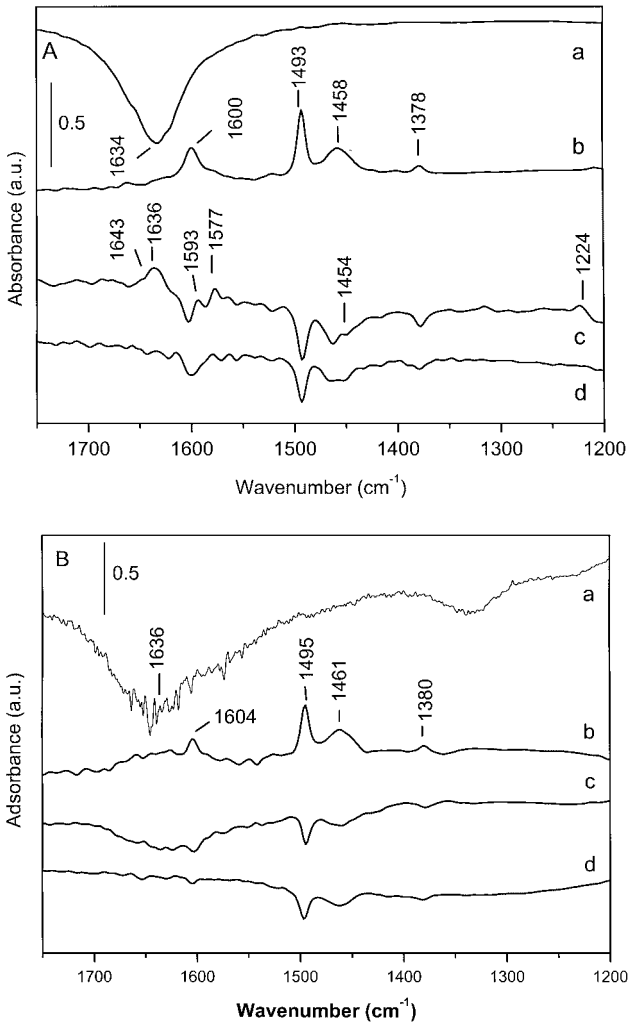

FIG. 7. IR difference spectra of W 19 (A) and TiO_2 (B) samples following treatments: (a) evacuation for 2 h at room temperature; (b) dosing of 5 Torr of toluene into the IR cell and subsequent introduction of 50 Torr of oxygen; (c) irradiation for 1 h; and (d) evacuation of the sample for 15 min.

any information from this part of the spectra, only the range between 1750 and 1200 cm^{-1} is depicted in the figure.

The room temperature outgassing of W 19 (Fig. 7A, spectrum a) produces a decrease in the broad band of adsorbed water centered at 1634 cm^{-1}. Upon toluene adsorption (Fig. 7A, spectrum b), narrow bands are formed at 1600, 1493, 1458, and 1378 cm^{-1} and attributed to adsorbed toluene (18). The subsequent irradiation of the sample (Fig. 7A, spectrum c) causes a decrease in the bands attributed to adsorbed toluene and the appearance of several weak bands at 1643, 1593, 1577, 1455, and 1224 cm^{-1}, which are attributed to adsorbed benzaldehyde on the catalyst surface (18–20). The irradiation also leads to a partial recovery of the band due to adsorbed water. This indicates that water is being produced and adsorbed during the irradiation process due to the complete mineralization of toluene molecules to CO_2 and H_2O upon visible excitation. The fact that the generated water band is much more intense than the benzaldehyde ones suggests that a significant amount of the photooxidized toluene is completely mineralized to CO_2 and H_2O, in agreement with selectivities observed in the reactivity measurements (Table 3). After a subsequent outgassing at 295 K (Fig. 7A, spectrum d) the toluene bands disappear but not those of benzaldehyde, which is indicative of the different energy of adsorption of these organic molecules.

On the other hand, the irradiation of TiO_2 with visible light (Fig. 7B spectrum c,) produced a decrease in the toluene bands, but there is little evidence of significant photooxidation reaction since only weak product bands (e.g., mainly from water) were formed during the irradiation process. The small intensity of product bands contrasts with the results from other TiO_2 specimens under UV-light excitation (18); however, the approximately one order of magnitude lower activity displayed under visible light irradiation makes comparisons difficult. A subsequent outgassing at 295 K (Fig. 7B, spectrum d) induces the desorption of toluene from the surface.

DISCUSSION

Physicochemical Characterization

The XRD spectra (Fig. 1) indicate the dominant presence of an anatase-type crystalline phase in all Ti–W binary oxide samples, the crystallinity of which decreases with W content. The additional presence of a minor contribution from the orthorhombic WO_3 phase is exclusively detected in the W 27 specimen. No significant alteration in the type and characteristics of the mentioned phases occurs during the photooxidation reaction. Raman spectroscopy (Figs. 3A and 3B) further supports the conclusions concerning the existence and stability of the mentioned crystalline phases, although a certain tendency to give less-intense Raman peaks after exposure to reactants is evident. The latter may be likely related to carbonaceous residues accumulated on the surface during the reaction. Therefore, based on the joint consideration of XRD and Raman data, the solubility limit of W in the anatase network (using the microemulsion preparation method) can be ascertained to be roughly 20 at.%.

On the other hand, XPS shows that cations are in Ti(IV) and W(VI) formal oxidation states in both fresh (calcined) and postreaction specimens, irrespective of the W content (Table 1). The absence of reduced (Ti (III) or W(V)) cationic states was further confirmed by using EPR spectra taken at 77 K (data not shown). This agrees with previous results from Ti–W mixed oxides (21). The stoichiometry of the mixed oxide is thus $Ti_{1-x}W_xO_{2+x}$. Such an $O/(Ti+W)$ ratio higher than 2.0 can, in principle, be accommodated in the anatase lattice in several ways. One would be the

appearance of interstitial O ions, in same number as that of W ions (which would be substituting for Ti ions in the octahedral cationic sites of the lattice). However, interstitial oxygen is unlikely to be in Ti oxide networks (22). The only other simple possibility is to have cation vacancies, one for every two W ions introduced substituting for Ti ions. Although this implies the disappearance of a number of Ti cation–O anion bonds, it is likely that the higher strength of W–O bonds (expected from the higher ionic charge of the W ions) will significantly compensate for this. Of course, complex defect combinations can be also envisaged. For example, it is known that the introduction of Fe^{3+} substituting for Mg^{2+} in MgO takes place by forming cation vacancies while other (Fe) cations are displaced to interstitial positions (providing a tetrahedral oxygen coordination around those cations), with all this occurring in defect associations of a specific configuration (the so-called Koch clusters (23)). Since the antase lattice is derived from that of MgO by suppressing 50% of its cations in a specific ordered way, one might consider also in our case the possible formation of similar cation interstitials/vacancy complexes. However, significant fractions of tetrahedral W interstitials are unlikely to be present here (at least for the W 14 and W 19 samples), since such species are expected to give specific Raman peaks (16), which have not been observed in these materials.

Therefore, the existence of a structure where the required MO_{2+x} stoichiometry is accommodated by only cationic site defects (cation vacancies and W^{6+} substituting for Ti^{4+}) seems the most likely one in these materials. Since the radii of both ions are very similar (0.605 Å for Ti^{4+}, 0.600 Å for W^{6+} (24)), one does not expect large length variations in the shorter cation–O bonds, which are nearly parallel to the (001) lattice plane, while the longer axial bonds, parallel to the *c* axis, leave room for shortening, which is likely to be promoted by the higher charge of the W ion. This, besides increasing the average cation–O bond strength, might provide an explanation for the observed shortening of the *c* axis, while the *a* axis length remains nearly constant upon an increase in W content. It should be noted, though, that shortening of the *c* axis has been observed in anatase also upon doping with Ca, Sr, and Ba (25), an effect which certainly must have a different origin since the types of defects expected are clearly not the same. Computer modeling and/or other experimental data (e.g., EXAFS measurements) might be required to clarify this point, which for the moment remains necessarily speculative. On the other hand, the fact that the observed *c* axis shortening occurs mainly for the higher W contents suggests the possible existence of a cooperative effect (defect association) in the region around/above 15 at.%.

Analysis of the presence of defects could be also performed by using the FWHM of the 144-cm^{-1} Raman peak (E_g Raman mode ascribed to the anatase structure; Fig. 4). On elimination of the contribution of the phonon confinement (reduced spatial correlation due to the nanostructure nature of the materials) (26) the net effect of vacancies to FWHM can be estimated to be ca. 7.5, 9, and 10 cm^{-1}, respectively, for samples with ca. 0–5, 15, and 20 at.% W. Both cationic and anionic vacancies should contribute to the broadening of the (E_g) Raman phonon mode due to (energy) potential fluctuations induced by them (27). In our case, it is possible to have also an additional effect of W presence in cation sites. Further analysis of these data would require knowledge of the relative distribution of different types of cation and defect sites and, as said before, lies outside of the scope of the present work.

The presence of W=O bonds at the surface of the Ti–W mixed oxides is evidenced by the Raman results (Figs. 3A and 3B). It is interesting that these bonds have a W–O stretching frequency with an appreciable shift to higher wavenumbers with respect to the W 3.4 TiO_2 reference sample. As is well known, a direct relationship can be established between the W–O stretch frequency and corresponding bond length (28), with the latter parameter being also related to the basic strength of the other W oxide ligands; the stronger the basic character of the "equatorial" oxide ligands, the weaker the W=O "axial" bond and the lower the W–O stretch frequency [29]. The different chemical environment of the mono–oxo wolframyl species which are either bonded/grafted to the surface of W-supported reference/Ti–W binary oxide specimens is then clearly manifested. The observed shift indicates a stronger W=O bond when W is located in anatase crystalline positions at surface shells. The corresponding weaker interaction with the remaining coordination oxygen would certainly modify the properties of surface hydroxyl groups (see below). On the other hand, XPS analysis (Fig. 5) suggests the absence of significant preferential surface segregation of any of the cations on Ti–W mixed oxides. Additionally, in the case of W 27, XPS indicates that the W fraction present as large WO_3 particles (detected by XRD) is not specifically at the surface of the Ti–W mixed oxide phase.

Therefore, concerning W insertion into the anatase network, we may thus conclude that our Ti–W samples do in fact contain substitutional Ti–W mixed oxides with a maximum W content of ca. 20 at.%. Roughly, W appears homogeneously distributed in the whole material, with no important concentration gradient between the bulk and the surface of the material.

The doping of anatase has several consequences to the properties of the mixed oxides. First, a decrease in primary particle size is detected (Table 1). This behavior has been already observed in Ca-, Sr-, and Ba-doped anatase (25), contrasts with the sintering process (and concomitant loss of surface area) favored in supported W–TiO_2 samples by coalescence during clacination (see Table 1 and Ref. (30)), and may be likely related to the type and number of point defects, the presence of which would limit particle growth

(upon calcination). The strong decrease in particle size occurring between samples with 15 and 20 at.% W, can be then associated with the mentioned increase in cationic vacancies and the above-mentioned possible ordering effect on the defect distribution. Further support of this conclusion can come from comparison with (anion vacancy containing) Ca-, Sr-, and Ba-doped anatase, where reduction in particle size is strong for doping levels below 5 at.% and varies only smoothly above such point (25).

The presence of W also has influence on the electronic properties of the Ti–W binary oxides. Figure 6 shows a progressive shift in the band gap absorption onset to the visible region with W content. In bare anatase, the absorption is associated with the O^{2-}–Ti^{4+} charge transfer corresponding to electronic excitation from the valence band (having dominant O 2p character) to the conduction band (Ti 3d character) (31). The similar energy of Ti 3d and W 5d levels would suggest that W substitutional doping in anatase only produces moderate widening of electronic bands (roughly similar crystal field splitting for both cations, just slightly differing in the *d* orbital average size) (31). However, the presence of donor levels close to the conduction band has been theoretically postulated (32), and their influence on the UV–vis spectra can be observed in Fig. 6. The electronic effects are, on the other hand, expected to become progressively more important concomitantly with the observed decrease in *c* cell parameter and volume (e.g., decreasing anion–cation bond distances) experienced by samples with a W content above 15 at.%. Indeed, such a lattice contraction may make both valence and conduction bands broader, decreasing the gap between them. It can be also noted that the W 3.4 TiO_2 sample also displays a redshift attributable to W-supported species, the magnitude of which is similar to that of the W 0.9 sample.

Catalytic Properties

Table 3 shows the reaction rates calculated for toluene mineralization; this parameter grows with the W content of the Ti–W mixed oxide, being moderately reduced when the additional presence of WO_3 phase is detected. The latter result can be qualitatively explained by taking into account the catalytic behavior displayed by the W single oxide prepared by microemulsion and also included in Table 3. Considering samples with exclusive presence of Ti–W mixed oxide, it can be noted that low-loaded W samples enhance moderately the reaction rate with respect to the parent pure-anatase sample, with the W 19 specimen giving the largest enhancement. The higher activity of the Ti–W samples can be also evidenced by the IR study (Fig. 7). After toluene adsorption, irradiation in the presence of oxygen mainly produces (in the experimental conditions) photodesorption of the organic for TiO_2 while in W 19 the presence of benzaldehyde (partial oxidation product and/or intermediate in total oxidation) and water (with CO_2 the products of the mineralization path) is detected in the infrared spectrum. Benzaldehyde appears, as mentioned, as a partial oxidation intermediate of the degradation process, as happens when using UV-light excitation for pure titania samples [18].

The differential behavior induced by the presence of W in the anatase structure may have chemical and/or physical grounds. In the first place, the adsorption of toluene displays subtle differences when comparing with IR the TiO_2 reference and the W 19 sample; in fact, a consistent redshift of 4 to 2 cm^{-1} is detected in all IR-active bands (Fig. 7). This probably indicates some differences between the hydroxyl groups present in both surfaces, although IR was unable to clarify the situation due to the broad and illresolved shape of the corresponding region of the spectrum during the experiments described in the previous section. The beneficial effect of W on the photoactivity of Ti–W samples has been, however, mainly explained in the literature by considering the formation of intermediate W(V) species by means of a transfer of photogenerated electrons (33, 34). This reduced W species could be oxidized to W(VI) by transferring electrons to oxygen (35) or by reaction with holes (h^+). Obviously, the first process is a chemical step of the degradation reaction while the second is one of the possible paths of the recombination process. The continuous growth of the reaction rate with W content (and the absence of segregation phenomena, which may alter surface W concentration with respect to nominal one) may in fact suggest that W mostly acts as an efficient charge trapping center when located at the surface, mainly influencing oxygen activation and not hydrocarbon one (EPR results) via next-nearest hydroxyls. Note, on the other hand, that Raman indicates that W-deposited reference and the Ti–W samples contain W cations with different interactions with neighboring oxygen, giving some support to the different reactivity of such W centers in the toluene mineralization. It must be stressed that the surface-W potential of being dominantly a (catalytically active) charge trapping or, on the contrary, a recombination electron-hole center is strongly dependent on the nanostructure form of the material. As was mentioned in the introduction, due to the minimization of the band bending, nanosize (or colloidal) materials can simultaneously transfer electron and holes to the surface, being then able to facilitate the attack on the reactants (of particular interest for our system is the attack on oxygen by reduced W centers) (11).

Finally, the remaining important term for explaining the photoactivity is related to the effect of the dopants in the existence of electronic impurity levels, which in the case of W are known to be close to the conduction band (3, 7, 32). Here, the presence of such W-induced electronic levels produces a redshift in the UV–vis spectra (Fig. 5), allowing a progressively larger power of absorption in the visible region in parallel to the growth of the W content. On the other hand, comparison between photoactivity of TiO_2 reference

and W 19 samples using UV- and sunlight-type excitation displays, respectively, a 1.6 to 3.3 ratio, giving support to the influence of electronic effects on the enhanced activity of toluene degradation using solar light. Nevertheless, it can be pointed out that in the case of our high-loaded samples (W 14 and W 19), a correlation can be observed between the concentration of surface, isolated W species detected by Raman and photocatalytic activity. In addition, the practical absence of such W species for the W 0.9 and W 3.4 TiO_2 samples is likely in the origin of the near constant reaction rate with respect to the TiO_2 reference system. Calibration of the relative importance of W-induced electronic vs surface charge trapping effects remains, however, to be verified. On the other hand, these results stress the importance of the preparation method, as this may allow the tuning of W surface concentration and chemical (isolated, polymeric, or aggregated species) distribution. Additionally, it controls the maximum concentration of W inserted into the anatase structure and thus the physical properties of the resulting solid.

CONCLUSIONS

In this work the synthesis of Ti–W mixed oxides with anatase structure have been pursued and samples containing up to ca. 20 at.% W mainly in substitutional positions in the mentioned anatase network were obtained. These materials do not display significant segregation of W and/or Ti to the surface of the solid. The substitutionally disordered Ti–W mixed oxide samples are nanosize materials and display a continuous enhanced photocatalytic activity in the degradation of toluene when increasing the percentage of W present in the anatase structure. This growth can be explained on the basis of the presence of W-related charge trapping centers at the surface of the material as well as of the electronic influence of W in the creation of electronic states in the (bare anatase) band gap and the concomitant decrease of the photoabsorption band gap energy onset. The charge trapping centers appear to have a nature different from those corresponding to W-supported samples. The study thus suggests that substitutionally disordered Ti–W binary mixed oxides having an anatase structure and high quantities of W may be more efficient photocatalysts in the degradation of toluene using sunlight-type excitation than are classic Ti-only based ones.

ACKNOWLEDGMENTS

The authors thank the "Ayuntamiento de Coslada" and CYCIT (project MAT2001-2112-CO2-O1) for financial support of this job.

REFERENCES

1. Serpone, N., and Pelizzetti, E., Eds., "Photocatalysis. Fundamental and Applications." Wiley, New York, 1989.
2. Hoffmann, M. R., Martin, S. T., Choi, W., and Bahnemann, D. W., *Chem. Rev.* **69**, 95 (1995).
3. Choi, W., Termin, A., and Hoffman, M. R., *Angew. Chem. Int. Ed.* **33**, 1091 (1994).
4. Brezová, V., Blazková, A., Karpinsky, L., Groskova, J., Havlínová, B., Jorík, V., and Ceppan, M., *J. Photochem. Photobiol. A* **109**, 177 (1997).
5. Anpo, M., *Stud. Surf. Sci. Catal.* **130**, 157 (2000).
6. Yamasita, H., Ichihashi, Y., Takeuchi, M., Kishiguchi, S., and Anpo, M., *J. Synchrotron Rad.* **6**, 451 (1999).
7. Cohen, M. M., "Introduction to the Theory of Semiconductors," 2nd ed., Gordon, Amsterdam, 1999.
8. Moser, J., Gratzel, M., and Galley, R., *Helv. Chim. Acta* **70**, 1056 (1987).
9. Fuerte, A., Hernández-Alonso, M. D., Maira, A. J., Martínez-Arias, A., Fernández-García, M., Conesa, J. C., and Soria, J., *Chem. Commun.* **2001**, 2178.
10. Schwuger, M.-J., Stickdorn, K., and Schomacker, R., *Chem. Rev.* **95**, 849 (1995).
11. Choi, W., Termin, A., and Hoffman, M. R., *J. Phys. Chem.* **98**, 13669 (1994).
12. Maira, A. J., Yeung, K. L., Soria, J., Coronado, J. M., Belver, C., Lee, C. Y., and Augugliaro, V., *Appl. Catal. B* **29**, 327 (2001).
13. Hesse, R., Chassé, T., and Szargan, R., *Fresenius J. Anal. Chem.* **365**, 48 (1999).
14. Burdett, J. K., *J. Am. Chem. Soc.* **109**, 3639 (1987).
15. Gutiérrez-Alejandre, A., Ramírez, J., and Busca, G., *Langmuir* **14**, 630 (1998).
16. Luca, V., Thomson, S., and Howe, R. F., *J. Chem. Soc. Faraday Soc.* **93**, 2195 (2000).
17. Wagner, C. D., Riggs, W. M., Davis, L. E., and Moulder, J. F., *in* "Handbook of X-Ray Photoelectron Spectroscopy" (G. E. Muilenberg, Ed.), pp. 68, 146. Perkin-Elmer, Minesota, 1978.
18. Maira, A. J., Coronado, J. M., Augugliaro, V., Yeung, K. L., Conesa, J. C., and Soria, J., *J. Catal.* **202**, 413 (2001).
19. Méndez-Román, R., and Cardona-Martínez, N., *Catal. Today* **40**, 353 (1998).
20. Martra, G., *Appl. Catal. A* **200**, 275 (2000).
21. Grzybowska, B., Sloczynsky, J., Grabowski, R., Samson, K., Gressel, I., Waislo, K., Genbembre, K., L., and Barteaux, Y., *Appl. Catal. A* **230**, 1 (2002).
22. Kofstad, P., "Nonstoichiometry, Diffusion, and Electrical Conductivity on Binary Mixed Oxides." Wiley, New York, 1972.
23. Koch, F., and Cohen, J. B., *Acta Crystallogr. B* **25**, 275 (1969).
24. Shannon, R. D., *Acta Crystallogr. A* **32**, 751 (1976).
25. Al-Salim, N. I., Bagshaw, S. A., Bittar, A., Kemmit, T., McQuillan, A. J., Mill, A. M., and Ryan, M. J., *J. Mater. Chem.* **10**, 2358 (2000).
26. Zhang, W. F., He, Y. L., Zhang, M. S., and Chen, Q., *J. Phys. D Appl. Phys.* **33**, 912 (2000).
27. Parayanthal, P., and Pollack, F. H., *Phys. Rev. Lett.* **52**, 1822 (1984).
28. Hardcastle, F. D., and Walchs, I. E., *J. Raman Spectrosc.*, **26**, 397 (1995).
29. Gutiérrez-Alejandre, A., Castillo, P., Ramírez, J., Ramis, G., and Busca, G., *Appl. Catal. A* **216**, 181 (2001).
30. Di Paola, A., Marci, G., Palmisano, L., Schiavello, M., Uosaki, K., Ikeda, S., and Ohtani, B., *J. Phys. Chem. B* **106**, 637 (2002).
31. Burdett, J. K., Hughbanks, T., Miller, G. J., Richarson, J. W., and Smith, J. V., *J. Am. Chem. Soc.* **109**, 3639 (1987).
32. Murata, Y., Fukuda, S., and Ishikawa, S., *Zairyoto Kankyo* **49**, 412 (2000).
33. Do, Y. R., Lee, W., Dwght, K., and World, A., *J. Solid State Chem.* **108**, 198 (1994).
34. Tennakone, K., Haperuna, O. A., Bandara, J. M., and Kiridena, W. C. B., *Semicond. Sci. Technol.* **7**, 423 (1992).
35. Marci, G., Palmisano, L., Sclafani, A., Venezia, A. M., Campostrini, R., Carturan, G., Martín, C., Rives, V., and Solana, G., *J. Chem. Soc. Faraday Trans.* **92**, 879 (1996).